PTEP

Prog. Theor. Exp. Phys. **2014**, 023A01 (11 pages)
DOI: 10.1093/ptep/ptt122

Bifurcation scenarios for a 3D torus and torus-doubling

Naohikio Inaba[1,*], Munehisa Sekikawa[2], Yoshimasa Shinotsuka[3], Kyohei Kamiyama[3], Ken'ichi Fujimoto[4], Tetsuya Yoshinaga[4], and Tetsuro Endo[3]

[1]*Organization for the Strategic Coordination of Research and Intellectual Property, Meiji University, 214-8571 Kawasaki, Japan*
[2]*Department of Mechanical and Intelligent Engineering, Utsunomiya University, 321-8585 Utsunomiya, Japan*
[3]*Department of Electronics and Bioinformatics, Meiji University, 214-8571 Kawasaki, Japan*
[4]*Institute of Health Biosciences, The University of Tokushima, 770-8509 Tokushima, Japan*
[*]E-mail: naohiko@yomogi.jp

Received October 23, 2013; Revised December 20, 2013; Accepted December 21, 2013; Published February 1, 2014

Bifurcation transitions between a 1D invariant closed curve (ICC), corresponding to a 2D torus in vector fields, and a 2D invariant torus (IT), corresponding to a 3D torus in vector fields, have been the subjects of intensive research in recent years. An existing hypothesis involves the bifurcation boundary between a region generating an ICC and a region generating an IT. It asserts that an IT would be generated from a stable fixed point as a consequence of two Hopf (or two Neimark–Sacker) bifurcations. We assume that this hypothesis may puzzle many researchers because it is difficult to assess its validity, although it seems to be a reasonable bifurcation scenario at first glance. To verify this hypothesis, we conduct a detailed Lyapunov analysis for a coupled delayed logistic map that can generate an IT, and indicate that this hypothesis does not hold according to numerical results. Furthermore, we show that a saddle-node bifurcation of unstable periodic points does not coincide with the bifurcation boundary between an ICC and an IT. In addition, the bifurcation boundaries of torus doubling do not coincide with a period-doubling bifurcation of unstable periodic points. To conclude, torus bifurcations have no relation with the bifurcations of unstable periodic points. Additionally, we exactly derive a quasi-periodic Hopf bifurcation boundary introducing a double Poincaré map.

Subject Index A30, A34

1. Introduction

The rapid increase of computational power enables us to numerically solve higher-dimensional dynamics [1–14,17,18]. In such high-dimensional dynamics, hyperchaos [5,10], torus-doubling [1,6,15,16], and a 3D torus can be generated [3,4,7–14,17–19] that cannot be observed in minimal-dimensional dynamics, which can generate chaos such as 3D autonomous ODEs, and 2D nonautonomous ODEs. In particular, bifurcations of low-dimensional quasi-periodic oscillations have been the subjects of intensive research in recent years [1–4,6–18]. There are two transition routes from a 2D torus to a 3D torus. Vitolo et al. called these transitions quasi-periodic Hopf (QH) bifurcations and quasi-periodic saddle-node (QSN) bifurcations [20]. However, significant bifurcation problems concerning torus bifurcations have remained unsolved. For example, Sekikawa et al. have recently discovered a bifurcation structure called "two-torus Arnold tongues" [10] in a three-LC resonant

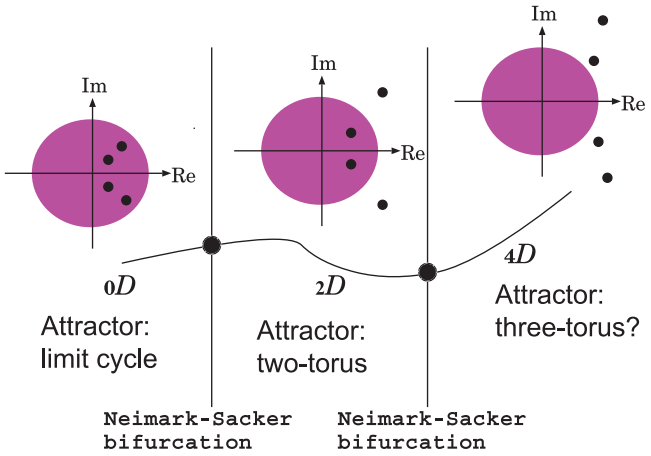

Fig. 1. Hypothesis concerning the bifurcation of a limit cycle to a 3D torus presented in Ref. [17].

oscillator. Two-torus Arnold tongues refer to a bifurcation structure in which two of the three independent frequency components of a 3D torus become rational, and exist similar to periodic states existing in a region generating a 2D torus in a conventional Arnold tongue. The two-torus Arnold tongues are observable in experimental measurements [10]. Anishchenko et al. [14] analyzed a 4D driven oscillator, and claimed that, by using a double Poincaré map, a QSN bifurcation of a 2D torus to a 3D torus occurs when a stable 2D torus and a saddle 2D torus merge together and disappear.

A precedent experiment on bifurcations of a 3D torus in 2000 shows, via a detailed conceptual diagram in Ref. [17], that the bifurcations of a 3D torus could occur from a limit cycle as a consequence of two Hopf (or two Neimark–Sacker) bifurcations. At first glance, their argument regarding the bifurcation structure seems to be reasonable. However, their scenario may puzzle many researchers because it may not be easy to verify the validity of their hypothesis. It was not easy to numerically check the hypothesis by computation a decade ago. We will indicate that the claim of Anishchenko et al. [14] appears to contradict the claim in Ref. [17] because the latter claim indirectly indicates that the bifurcation boundary between a 2D torus and a 3D torus occurs when a saddle-node (SN) bifurcation of an unstable periodic solution is generated, which is explained in detail below.

We assume that the objective dynamics is a 4D Poincaré map or 4D discrete dynamics. Additionally, we assume that the four eigenvalues are two pairs of complex-conjugates on the complex plane. Figure 1 shows the position of the four eigenvalues. The abscissa denotes a bifurcation parameter. In the figure, a region denoted by ${}_iD$ is an area where a fixed point (or periodic points), of which the instability dimension is i, exists [21,22]. Therefore, the region denoted by ${}_0D$ is an area where a stable fixed point exists, as illustrated in the left picture in Fig. 1. Moving the bifurcation parameter from left to right, a Neimark–Sacker (NS) bifurcation occurs when a pair of complex-conjugate eigenvalues cross the unit circle. It is well known that this bifurcation is identified with a transition from a limit cycle to a 2D torus. The issue presented in Ref. [17] is the point at which the second NS bifurcation of the limit cycle would coincide with the bifurcation boundary from a 2D torus and a 3D torus, i.e., whether the region marked ${}_4D$ generates an IT. It would hold at first glance. However, no one has investigated the scenario in Fig. 1 by illustrating the bifurcation diagrams.

The reason that the claim in Ref. [17] contradicts the claim of Anishchenko et al. [14] is explained as follows. A periodic solution can bifurcate to a 2D torus by an SN bifurcation, as well as an NS

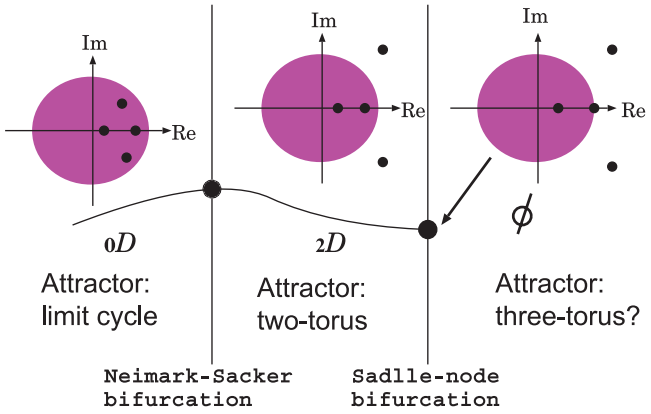

Fig. 2. Another hypothesis for the bifurcation boundary between a 2D torus and a 3D torus deduced from the hypothesis illustrated in Ref. [17].

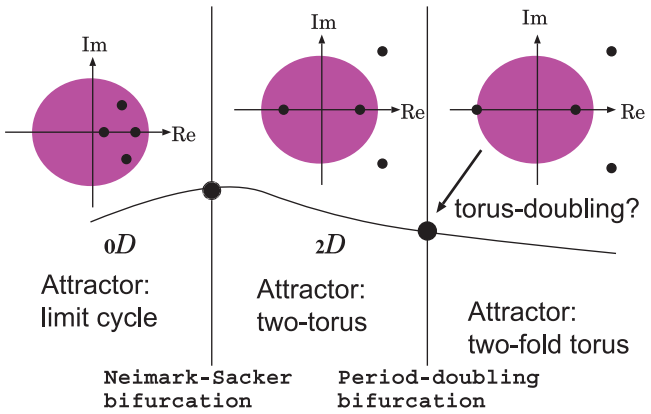

Fig. 3. Relation between the torus-doubling and period-doubling bifurcations of unstable periodic points.

bifurcation. If the 2D torus bifurcates to a 3D torus through a second Hopf (or a second NS) bifurcation as illustrated in Fig. 1, it will be deduced that the 2D torus would bifurcate to a 3D torus through an SN bifurcation of an unstable periodic solution, as illustrated in Fig. 2. However, Anishchenko et al. [14] claims that the QSN bifurcation occurs when a 2D torus attractor and a saddle 2D torus merge together and disappear by an SN bifurcation.

In this study we conduct a Lyapunov analysis on a coupled delayed logistic map, which is a simple diffeomorphism that can generate a 2D invariant torus (IT) corresponding to a 3D torus in vector fields, and indicates that the hypothesis for the generation of an IT in the two cases presented in Figs. 1 and 2 appears to be invalid.

Additionally, a similar bifurcation problem for torus-doubling arises from the position of four eigenvalues, i.e., whether torus-doubling bifurcation points coincide with period-doubling bifurcation points of unstable periodic points. The position of the four eigenvalues is presented in Fig. 3. It is well known that, if the periodic points are stable, a period-doubling bifurcation is generated when a real eigenvalue crosses -1. However, according to our numerical results, their bifurcation parameter values do not coincide. To conclude, torus bifurcations have no relation with those of unstable periodic solutions.

Lastly, we attempt to derive an exact bifurcation boundary between a region generating an ICC and a region generating an IT caused by a QH bifurcation, which is a major bifurcation from an

ICC to an IT. Because quasi-periodic attractors with n-incommensurate frequency components are represented by a form of an n-dimensional torus in vector fields, an ICC on the Poincaré section becomes a fixed point on the double Poincaré section, and an IT becomes an ICC on this section. Therefore, we can derive the QH bifurcation boundary exactly by detecting the attractor on the double Poincaré section. This is a typical method. We derived the QH bifurcation boundary with an accuracy of 10^{-5}, and verified that it coincides with the boundary obtained via Lyapunov analysis. We can clearly observe an ICC on the double Poincaré section corresponding to a 3D torus in vector fields.

2. Analysis of a coupled delayed logistic map generating IT

In this study, we numerically investigate a coupled delayed logistic map in the following form, wherein F is a simple differmorphism:

$$\begin{aligned} F(x_n, y_n, z_n, w_n)^\top : \quad & x_{n+1} = y_n, \\ & y_{n+1} = B_1 y_n (1 - x_n) + \varepsilon_1 w_n, \\ & z_{n+1} = w_n, \\ & w_{n+1} = B_2 w_n (1 - z_n) + \varepsilon_2 y_n. \end{aligned} \tag{2.1}$$

Since we analyze the discrete-time dynamical system in this study, we use the terms "1D invariant closed curve" (ICC) and "2D invariant torus" (IT) instead of "2D torus in vector fields" and "3D torus in vector fields."

Because of the simplicity of a delayed logistic map, an NS bifurcation parameter value of B_1 ($\varepsilon_1 = \varepsilon_2 = 0$) is manually calculated as $B_1 = 2$. Since a delayed logistic map can generate an ICC, a coupled delayed logistic map can generate an IT. This coupled map is an appropriate representation of the dynamics for verifying the hypothesis presented in Fig. 1 because it generates a stable fixed point in a region ${}_0D$, an ICC in ${}_2D$, and an IT in ${}_4D$, respectively, when $\varepsilon_1 = \varepsilon_2 = 0$, i.e., the hypothesis holds when the coupling parameters are zero. If the structure is stable for positive ε_1 and ε_2, the hypothesis presented in Fig. 1 holds. If the structure is destroyed for positive ε_1 and ε_2, then the hypothesis is wrong.

We conduct a Lyapunov analysis for Eq. (2.1), and illustrate the results via several two-parameter bifurcation diagrams. In actual calculations of Lyapunov spectra, we employ an algorithm presented by Shimada and Nagashima [23]. Specifically, we derive the approximated Lyapunov exponents using the following equations:

$$\begin{aligned} \lambda_1 &\simeq \frac{1}{N} \sum_{j=M+1}^{M+N} \ln ||DF_j e_1^j||, \\ \lambda_1 + \lambda_2 &\simeq \frac{1}{N} \sum_{j=M+1}^{M+N} \ln ||DF_j e_1^j \times DF_j e_2^j||, \\ \lambda_1 + \lambda_2 + \lambda_3 &\simeq \frac{1}{N} \sum_{j=M+1}^{M+N} \ln ||DF_j e_1^j \times DF_j e_2^j \times DF_j e_3^j||, \\ \lambda_1 + \lambda_2 + \lambda_3 + \lambda_4 &\simeq \frac{1}{N} \sum_{j=M+1}^{M+N} \ln ||DF_j e_1^j \times DF_j e_2^j \times DF_j e_3^j \times DF_j e_4^j||, \end{aligned} \tag{2.2}$$

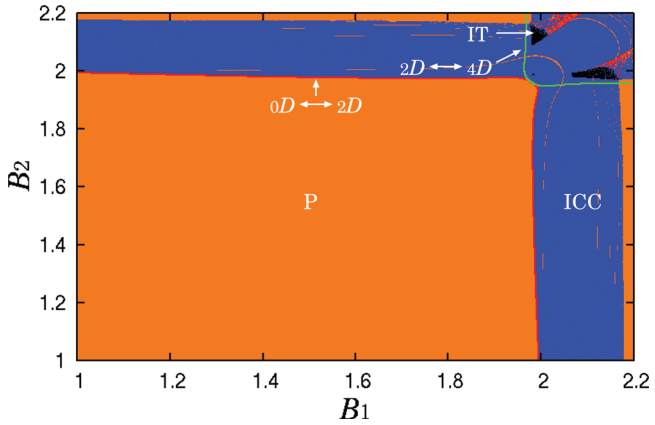

Fig. 4. Global two-parameter bifurcation diagram with $\varepsilon_1 = 0.025$ and $\varepsilon_2 = 0.035$.

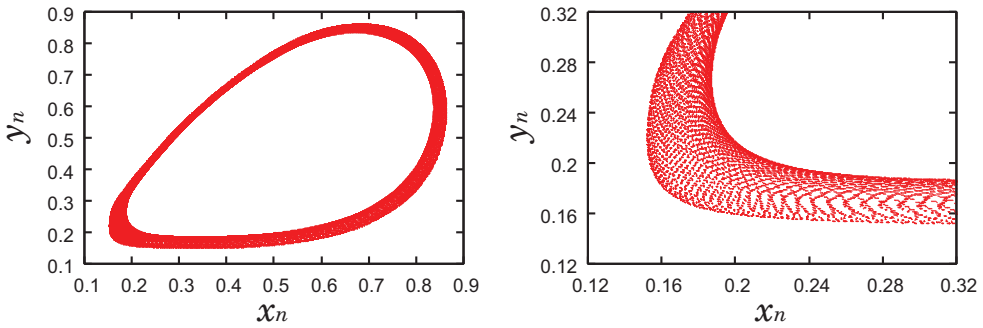

Fig. 5. A stable IT. (a) Left: a global picture with $B_1 = 2.1$, $B_2 = 2.0$, $\varepsilon_1 = 0.025$, and $\varepsilon_2 = 0.035$. (b) Right: a magnified view of (a).

where DF_j is a Jacobian matrix of F_j and e_i ($i = 1$, 2, 3, and 4) are orthonormal bases determined using the procedure outlined in Ref. [23]. It is known that the following relationship holds:

$$\lambda_1 \geq \lambda_2 \geq \lambda_3 \geq \lambda_4. \tag{2.3}$$

We count the number of zero Lyapunov exponents for each parameter value, and draw a bifurcation diagram. In the following discussion, we set $N = M = 1\,000\,000$ and assume $\lambda_i = 0$ if $|\lambda_i| < 1/100\,000$.

In the following discussion, we set $\varepsilon_1 = 0.025$ and $\varepsilon_2 = 0.035$. Figure 4 shows the global picture of the two-parameter bifurcation diagram. We use orange, blue, and black to indicate stable periodic points, an ICC, and an IT, respectively. The red line denotes the boundaries between regions generating a fixed point and regions generating ICCs. In addition, the green line indicates the boundary between ${}_2D$ and ${}_4D$. In the figure, red shaded areas indicate chaos-generating regions. A stable IT is depicted in Fig. 5.

First, we discuss the NS bifurcation of the fixed point denoted by the red line. Figure 6 shows a magnified view of Fig. 4 near the NS bifurcation of ${}_0D$. Figure 6 shows that the NS bifurcation boundary between ${}_0D$ and ${}_2D$ denoted by the red line completely coincides with the boundary between the fixed-point-generating region and an ICC-generating region. The red line is derived using a shooting algorithm defined in Ref. [21]. This is a well known bifurcation transition boundary from a stable periodic solution to a 2D torus in vector fields. The numerical result shows that the iteration numbers $M = 1\,000\,000$ and $N = 1\,000\,000$ are sufficient to detect the bifurcation boundary. It can be

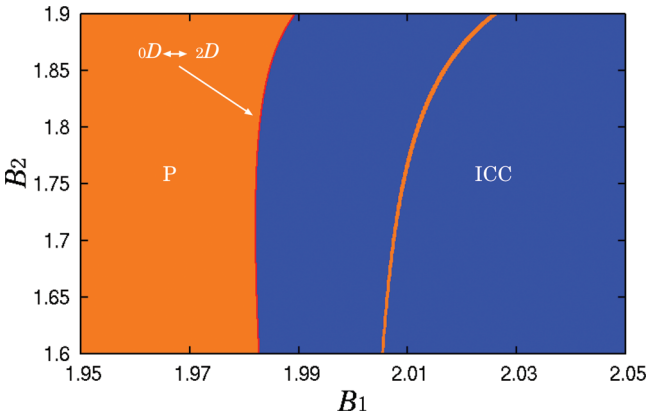

Fig. 6. Magnified view of the bifurcation diagram of Fig. 4 near the boundary between ${}_0D$ and ${}_2D$ with $\varepsilon_1 = 0.025$ and $\varepsilon_2 = 0.035$.

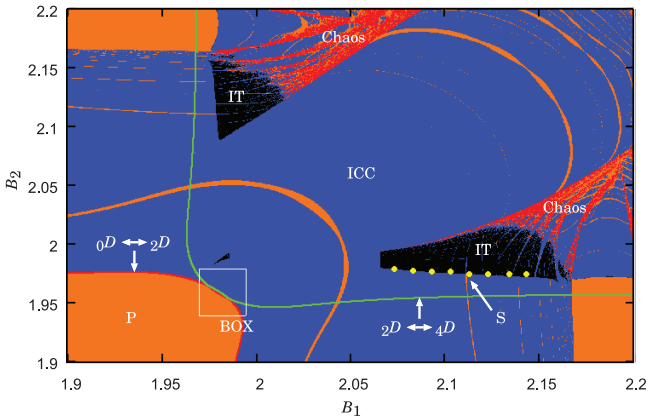

Fig. 7. Magnified view of the bifurcation diagram near the transition ${}_2D \leftrightarrow {}_4D$ with $\varepsilon_1 = 0.025$ and $\varepsilon_2 = 0.035$.

confirmed that our code used to calculate Eq. (2.2), and the code to draw the NS bifurcation curve using the shooting algorithm [21], are correct.

Next, we discuss the relation between the transition from an ICC to an IT and the NS bifurcation boundary from ${}_2D$ to ${}_4D$, which is a major theme of this study. A magnified view of the bifurcation diagram near the transition from ${}_2D$ to ${}_4D$ is illustrated in Fig. 7. From the figure, we find that an IT-generating region is divided into two domains, and furthermore, it becomes clear that the NS bifurcation of ${}_2D$ to ${}_4D$ does not coincide with the bifurcation boundary between an ICC and an IT. Therefore, according to the numerical results, the hypothesis in Fig. 1, stated in Ref. [17], is invalid for positive ε_1 and ε_2 in this discrete dynamics. In the figure, the solid yellow circles denote an exactly derived QH bifurcation boundary, the derivation of which is explained in Sect. 4.

We explain how the bifurcation diagram near the codimension-two bifurcation point existing at $B_1 = B_2 = 2$ with $\varepsilon_1 = \varepsilon_2 = 0$ changes for small positive ε_1 and ε_2. Figure 8 shows the bifurcation diagram near $B_1 = B_2 = 2$ for $\varepsilon_1 = 0.025$ and $\varepsilon_2 = 0.035$. It is confirmed again that the bifurcation boundary between ${}_0D$ and ${}_2D$ is the boundary between a stable fixed point and an ICC. However, the bifurcation boundary between ${}_2D$ and ${}_4D$ and the generation of an IT have no relation.

Next, we show that the hypothesis illustrated in Fig. 2 also appears to be wrong. Since a periodic solution exists in an ICC-generating region near an IT, indicated by S in Fig. 7, we show a magnified

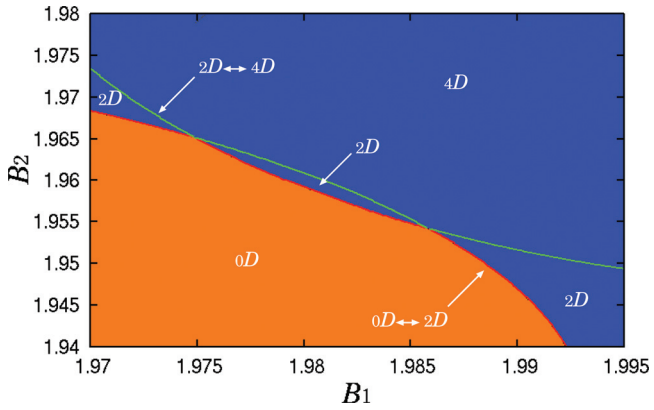

Fig. 8. Magnified view of the bifurcation diagram near the codimension-two bifurcation point with $\varepsilon_1 = 0.025$ and $\varepsilon_2 = 0.035$.

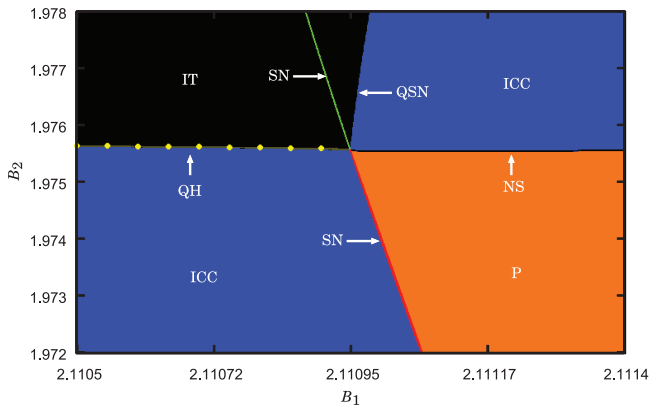

Fig. 9. Two-parameter bifurcation diagram near a saddle-node bifurcation with $\varepsilon_1 = 0.025$ and $\varepsilon_2 = 0.035$.

view of the bifurcation diagram in Fig. 9. In this figure, stable-periodic-solution-, ICC-, and IT-generating regions are observed.

It has been shown that a bifurcation boundary, denoted by a red line in Figs. 6 and 8, is an NS bifurcation of a stable periodic solution. In contrast, the red line illustrated in Fig. 9 is an SN bifurcation curve of a stable periodic solution, which is also derived in the procedure shown in Ref. [21]. Moving upward along the bifurcation line, one sees that the SN bifurcation curve of a stable periodic point can be traced further, and it transitions to an SN bifurcation curve of an unstable periodic solution, denoted by a green line. The SN bifurcation curve denoted by the red line coincides with the bifurcation boundary between a region generating a periodic solution and a region generating a stable ICC. However, the bifurcation boundary of the SN bifurcation curve of unstable periodic points, denoted by the green line, is not a bifurcation boundary between an ICC and an IT, which is similar to the case illustrated in the hypothesis of Fig. 1. Therefore, the hypothesis illustrated in Fig. 2 is also invalid.

In the figure, QH is a QH bifurcation boundary, and the yellow solid circles are an exactly derived QH bifurcation boundary, the derivation of which is explained in detail in Sect. 4.

The bifurcation boundary between an ICC-generating and an IT-generating region, denoted by "QSN" in Fig. 9, may be caused by an SN bifurcation of a stable ICC and a saddle ICC from the assertion by Anishchenko et al. [14].

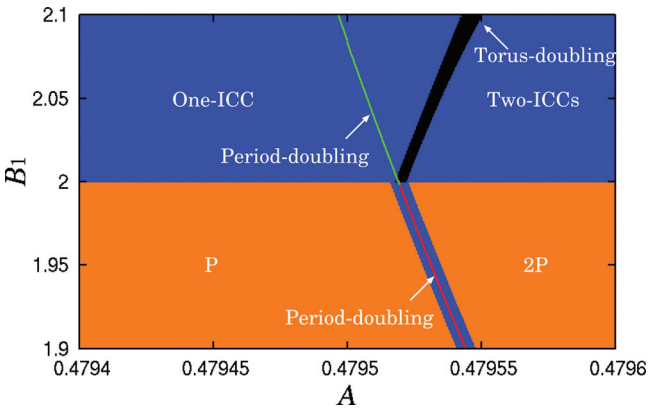

Fig. 10. Two-parameter bifurcation diagram near period-doubling and torus-doubling bifurcations with $\varepsilon_1 = 0.001$, $\varepsilon_2 = 0.002$, and $B_2 = 0.2$.

3. Relation between torus-doubling and period-doubling bifurcations of unstable periodic points

Herein, we investigate a bifurcation boundary of torus-doubling. Although it is not a bifurcation transition problem between an ICC and an IT, a similar hypothesis about the relations between torus-doubling and period-doubling bifurcations of unstable periodic points could arise from the position of the eigenvalues on the complex plane illustrated in Fig. 3. We conclude that the torus-doubling bifurcation boundary does not coincide with the period-doubling bifurcation boundaries of the unstable periodic points that are generated when one of the real eigenvalues crosses -1.

Since we cannot easily observe torus-doubling in the coupled two-delayed logistic map given by Eq. (2.1), we consider a coupled delayed logistic map and a Hénon map, given as follows:

$$\begin{aligned} G(x_n, y_n, z_n, w_n)^\top : \quad & x_{n+1} = y_n, \\ & y_{n+1} = B_1 y_n (1 - x_n) + \varepsilon_1 w_n, \\ & z_{n+1} = w_n + A z_n^2 + \varepsilon_2 y_n, \\ & w_{n+1} = B_2 z_n. \end{aligned} \tag{3.1}$$

Since the Hénon map generates period-doubling bifurcations, torus-doubling can occur in Eq. (3.1) under appropriate conditions.

To numerically derive the period-doubling and torus-doubling bifurcation boundaries by Lyapunov analysis, we distinguish them by colors in the bifurcation diagram, similar to the method used in Figs. 4–9 but replacing DF by DG in Eq. (2.2). Hence, we draw the period-doubling bifurcation curves with thin blue lines, and the torus-doubling bifurcation curves in black. However, it is difficult to illustrate the bifurcation boundaries with sufficiently thin lines. $N = 1\,000\,000$ is insufficient. Therefore, we set $N = 10\,000\,000$ and color the figure when $|\lambda| < 3/10\,000\,000$. The reader may feel that it is still not thin enough when studying the bifurcation diagram. However, it is beyond our computational ability to compute more than these iterations.

Figure 10 shows the two-parameter bifurcation diagram illustrated as mentioned above. We set $\varepsilon_1 = 0.001$, $\varepsilon_2 = 0.002$, and $B_2 = 0.2$. In the figure, the abscissa denotes the parameter A, and the ordinate is parameter B_1. Since the coupling parameters ε_1 and ε_2 are small, Eq. (3.1) can generate torus-doubling, and the boundary between the periodic-solution-generating and 2D-torus-generating regions is approximately $B_1 \simeq 2$ because the single delayed logistic map generates an NS bifurcation

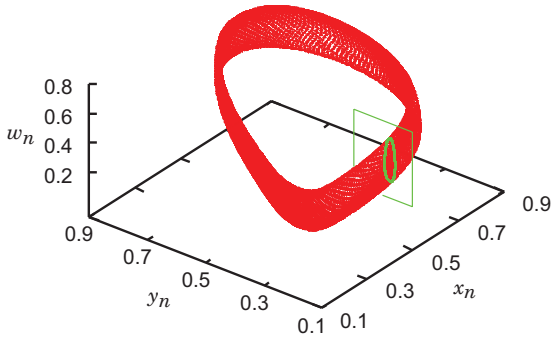

Fig. 11. Definition of a double Poincaré section.

if $B_1 = 2$. In the figure, the red line denotes the first period-doubling line, which is derived by a procedure presented in Ref. [21]. In this figure, the bifurcation boundary, denoted by a red line, coincides with a somewhat thick bifurcation boundary, obtained by Lyapunov analysis between the regions marked P and 2P. However, moving up the red line, it is continuously connected to the green line around $B_1 \simeq 2$. This is a period-doubling bifurcation curve of unstable periodic points. The thick black curve is the bifurcation boundary obtained by Lyapunov analysis between a 1D ICC and a second 1D ICC that consists of the two ICCs. The black curve does not coincide with the periodic-doubling bifurcation curve of unstable periodic points. Therefore, the scenario illustrated in Fig. 3 is also invalid.

4. Derivation of a QH bifurcation boundary

We now focus on the QH bifurcation boundary generated by Eq. (2.1). The QH bifurcation is a major transition from an ICC to an IT. We attempt to derive this bifurcation boundary by introducing a double Poincaré section. Because quasi-periodic attractors with n-incommensurate frequency components are represented by a form of an n-dimensional torus in vector fields, an ICC on the Poincaré map becomes a fixed point on the double Poincaré section, and an IT becomes an ICC on this section. Therefore, we can derive a QH bifurcation boundary exactly by detecting the attractor on the double Poincaré section.

We define the double Poincaré map as follows (see Fig. 11):

$$T : D \longrightarrow D, (x_0, y_0, z_0, w_0)^\top \mapsto (x_1, y_1, z_1, w_1)^\top \tag{4.1}$$

where $D = \{(x_n, y_n, z_n, w_n) | |x_n - 0.5| < 10^{-6},\ y_n < 0.5\}$. Because the domain of the double Poincaré section has a very small width, it is also called a double Poincaré slice. The attractors on the double Poincaré section projected onto the z_n–w_n plane are illustrated in Figs. 12(a) and (b). Because an approximated fixed point exists on T in the former case, this is a 2D torus in vector fields. In contrast, an IT forms an ICC on T. We can observe a clear ICC in Fig. 12(b). Therefore, by using the bisection method, the boundary between a region generating an ICC and a region generating an IT can be derived. The solid yellow circles in Figs. 7 and 9 denote the QH bifurcation boundary obtained with an accuracy of 10^{-5}. They can be seen on the bifurcation boundary between the blue and black zones.

Conversely, an IT can be generated by QSN bifurcations [20], which could occur by saddle-node bifurcations of a stable ICC and a saddle ICC [14]. Independently, this bifurcation may also be called a saddle-node-invariant-circle bifurcation in a certain field, and has been extensively studied [24]. QNS

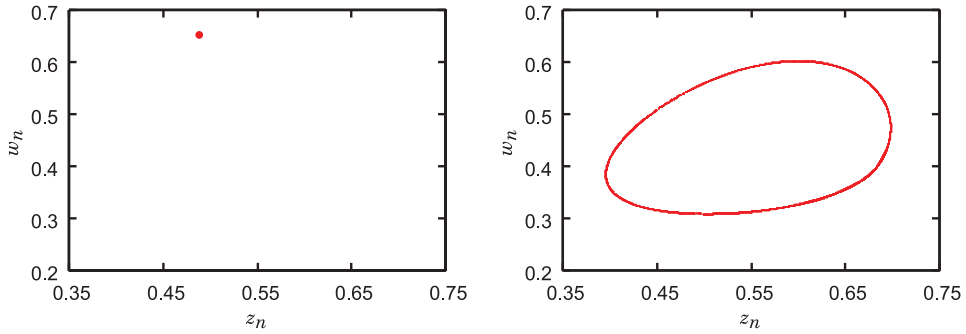

Fig. 12. Attractors on the double Poincaré section. (a) Left: a stable fixed point corresponding to a 2D torus in vector fields with $\varepsilon_1 = 0.025$, $\varepsilon_2 = 0.035$, $B_1 = 2.0$, and $B_2 = 2.0$. (b) Right: a stable ICC corresponding to a 3D torus in vector fields with $\varepsilon_1 = 0.025$, $\varepsilon_2 = 0.035$, $B_1 = 2.1$, and $B_2 = 2.0$.

bifurcations attract much attention because they lead to complex bifurcation structure. The bifurcation structure called two-torus Arnold tongues may be caused by QSN bifurcations [10]. However, the whole aspect of these phenomena has not yet become clear. Catching saddle 2D tori [25,26] could be the first step towards clarifying the complex bifurcation structure caused by QSN bifurcations.

5. Conclusion

An existing hypothesis states that an ICC bifurcates to an IT through an NS bifurcation of an unstable fixed point. According to sufficient numerical simulations, we have shown that this hypothesis is invalid. Furthermore, the bifurcation boundary between an ICC and an IT does not coincide with an SN bifurcation point of unstable periodic points. In addition, the torus-doubling bifurcation point did not coincide with a period-doubling bifurcation curve of unstable fixed points. Therefore, all the bifurcations of unstable periodic points have no relation with torus bifurcations. In addition, we have exactly derived a QH bifurcation boundary by introducing a double Poincaré section, and confirmed that these bifurcation points lie on the bifurcation boundary obtained by Lyapunov analysis. To show that an IT is generated exactly by an SN bifurcation of a stable ICC and a saddle ICC could be an avenue for further research.

Acknowledgements

This work was supported by MEXT/JSPS KAKENHI Grant Number 24560556.

References

[1] K. Mitsubori and T. Saito, IEEE Trans. Circuits Syst. I **41**, 782 (1994).
[2] N. Inaba, Y. Nishio, and T. Endo, Physica D **240**, 903 (2011).
[3] O. Hess, D. Merbach, H. Herzel, and E. Schöll, Phys. Lett. A **194**, 289 (1994).
[4] T. Saito and Y. Matsumoto, IEEE Trans. Circuits Syst. I **41**, 754 (1994).
[5] T. Suzuki and T. Saito, IEEE Trans. Circuits Syst. I **41**, 876 (1994).
[6] P. Ashwin and J. W. Swift, Int. J. Bifurc. Chaos **5**, 231 (1995).
[7] J. M. Lopez and F. Marques, Phys. Rev. E **68**, 036320 (2003).
[8] J. M. Lopez and F. Marques, Phys. Rev. Lett. **85**, 972 (2000).
[9] C. Giberti and R. Zanasi, Physica D **65**, 300 (1933).
[10] M. Sekikawa, N. Inaba, T. Tsubouchi, and K. Aihara, Physica D **241**, 1169 (2012).
[11] N. Inaba, M. Sekikawa, and T. Endo, IEICE NOLTA **3**, 508 (2012).
[12] D. J. Albers and J. C. Sprott, Physica D **223**, 194 (2006).
[13] H. T. Moon, P. Huerre, and L. G. Redekopp, Phys. Rev. Lett. **49**, 458 (1982).
[14] V. Anishchenko, S. Nikolaev, and J. Kurths, Chaos, **18**, 037123 (2008).

[15] V. Anishchenko and S. Nikolaev, Tech. Phys. Lett. **31**, 858 (2005).
[16] V. Anishchenko, *Dynamical Chaos-Models and Experiments: Appearance Routes and Structure of Chaos in Simple Dynamical Systems* (World Scientific, Singapore, 1995).
[17] R. Alaggio and G. Rega, Physica D **137**, 70 (2000).
[18] I. Manimehan, K. Thamilmaran, and P. Philominathan, Int. J. Bifurc. Chaos **21**, 1987 (2011).
[19] T. Yoshinaga and H. Kawakami, Codimension-two bifurcation in a forced oscillator. In *Dynamical Systems and Chaos*, eds. K. Shiraiwa, N. Aoki, and Y. Takahashi (World Scientific, Singapore, 1995).
[20] R. Vitolo, H. Broer, and C. Simó, Reg. Chaotic Dyn. **16**, 154 (2011).
[21] H. Kawakami, IEEE Trans. Circuits Syst. **31**, 248 (1984).
[22] H. Kawakami and T. Yoshinaga, Codimension two bifurcation and its computational algorithm. In *Bifurcation and Chaos: Theory and Applications*, ed. J. Awrejcewicz (Springer, Berlin, 1995).
[23] I. Shimada and T. Nagashima, Prog. Theor. Phys. **61**, 1605 (1979).
[24] S. Altmeyer, Y. Do, F. Marques, and J. M. Lopez, Phys. Rev. E, **86**, 046316 (2012).
[25] U. Feudel, C. Grebogi, and E. Ott, Phys. Rep. **290**, 11 (1997).
[26] K. Kamiyama, M. Komuro, and T. Endo, Int. J. Bifurc. Chaos **22**, 1250309 (2012).